Int. J. Electrochem. Sci., 12 **(2017)** 2658 – 2668, doi: 10.20964/2017.04.30

International Journal of
ELECTROCHEMICAL
SCIENCE
www.electrochemsci.org

A High Sensitive Electrochemical Avian Influenza Virus H7 Biosensor Based on CNTs/MoSx Aerogel

Jingzhi Tian[*], *Dandan Wang*, *Yongjie Zheng*, *Tao Jing*

Schoole of Chemistry and Engineering, Qiqihar University, Qiqihar, 161006, China;
[*]E-mail: zyj1964@163.com

Received: 30 October 2016 / *Accepted:* 8 February 2017 / *Published:* 12 March 2017

The three-dimensional CNTs/MoS_x aerogel was successfully prepared via solvothermal method. The favourable combination of MoS_2 material and 3D conductive networks of CNTs aerogel have created a sufficient active site for fast charge transport. The electrochemical immunosensor with a sandwich-type immunoassay using CNTs/MoS_x aerogel as trace labels was constructed. Avian influenza virus H7 (AIV H7) could be quantified sensitively using the proposed immunosensor. The immunoassay was carried out on the modified surface of CNTs/MoS_x with the adsorption of H7-polyclonal antibodies (PAb-CNTs/MoS_2). The immunosensor with PAb-CNTs/MoS_x as detection antibodies have demonstrated a linear detection range of 1-25 ng/mL with the low detection limit of 0.43 ng/mL.

Keywords: CNTs aerogel; Molybdenum sulfide; Electrochemical immunosensor; Avian influenza virus H7

1. INTRODUCTION

Avian influenza virus (AIV) H7 infections have occurred very often and caused many deaths since its observance at 1959. During the 1999-2000, infectious diseases caused by AIV H7N1 had spreading among poultry in Italy. Besides, the spread of infectious diseases resulted from AIV H7N7 were serious among both the poultry and people in the Netherlands [1]. What's worse, a new AIV H7N9 virus was first identified in China in March 2013, leading to the reported 165 deaths among 450 human cases of H7N9 infection [2].

To prevent and control the potential AIV H7 outbreaks, both the rapid diagnosis of AIV H7 virus and the construction of time-monitoring system are of great importance. Currently, several

methods including reverse transcription loop-mediated isothermal amplification (RT-LAMP) [3], polymerase chain reaction (PCR)-based assays [4, 5], nucleic acid sequence-based amplification (NASBA) [6] and enzyme-linked immunosorbent assays (ELISAs) [7] have been developed for AIV H7 detection. However, these detection methods still have many disadvantages which hinder the practical applications.

For the last few years, the electrochemical immunosensors have drawn worldwide attention owing to a great many advantages including power-saving, low cost and high sensitivity. Besides, the sensors are highly compatible with advanced micromachining technologies [8, 9]. For the electrochemical immunosensors, the typically used capture probe was antigens/antibodies. The presented weak electrochemical behavior of antigens/antibodies probe has greatly promoted the development of a bioactive enzyme-labeled method involved in the electrochemical immunosensor [10, 11]. Nevertheless, owing to the high activity, the employed enzyme is usually unstable. Silver nanoparticles, a category of metal nanoparticles with excellent electrochemical activity in a long time at room temperature, have been developed as labels to enhance the performance of immunosensor [12, 13]. Nevertheless, the detection antibody labeled by silver nanoparticles merely exhibited low sensitivity, leading to the urgent demand of a new trace label [13, 14].

Nanostructured molybdenum sulfide (MoS_x, $x \approx 2$ to 3) with S^{2-} or S_2^{2-} ligands can be used in various fields such as lithium ion batteries, catalysts and transistors [15-17]. In addition, molybdenum sulfide has demonstrated the possibility as an efficient catalytic support [18-20]. Owing to the increase of the electroactive surface area, the catalytic activity of the electrodes based on 3D porous materials can be greatly improved [21, 22]. Compared with conventional carbon materials, the 3D carbon materials with high surface area have exhibited the enhancement of electrical conductivity that is beneficial for electron transfer [23, 24]. Herein, a MoS_x/MWNTs nanocomposite was prepared by simply incorporating MoS_x into CNT aerogel through the solvothermal method. Then, monoclonal antibodies (MAbs) were immobilized using the as-prepared composite. What's more, MoS_x/MWCNTs were employed to modify polyclonal antibodies (PAbs) for the construction of electrochemical immunosensors.

2. EXPERIMENTS

2.1. Materials

Hydrochloroauric acid ($HAuCl_4$), 1-ethyl-3-(3-dimethylaminopropyl) carbodiimide hydrochloride (EDC), N-hydroxysuccinimide-activated hexa-(ethylene glycol) undecane thiol (NHS), $(NH_4)_2MoS_4$ powder, DMF and H_2SO_4 were supplied by Sigma-Aldrich. Pt/C (20 wt% Pt on Vulcan XC-72R) and Nafion (5 wt%) were purchased from DUPONT. The multi-walled carbon nanotubes (MWNTs) were obtained from CNano Technology Company Ltd. Bovine serum albumin (BSA) was obtained from Beijing Dingguo Biotechnology Co., Ltd (China). H7 antibodies were supplied by

Abcam (Cambridge, UK). All chemicals and materials were directly used after purchase. The water used in the entire experiments was purified using a Millipore system.

2.2 Preparation of AuNPs-CNTs/MoS_x nanocomposite

The CNTs/MoS_x aerogel was prepared by a solvothermal method [25]. Firstly, $(NH_4)_2MoS_4$ powder (220 mg), MWNTs aerogel (45 mg) and DMF (15 mL) were mixed into a 20 mL Teflon autoclave. In order to obtain a homogeneous solution, the mixture was treated with ultrasound for about 10 min at 25◦C. Then the solution was heated at 200◦C for 10 h. After cooling down, the reaction solution was centrifuged at 8000 rpm for 5 min and the obtained product was then washed with DI water for at least 5 times in order to get rid of DMF residuals and unreacted reactants. Finally, the CNTs/MoS_x aerogel was successfully prepared. To prepare the pure MoS_x particles without CNTs aerogel support, the exactly same procedure was used without the addition of MWNTs aerogel. Subsequently, the gold nanoparticle-CNTs/MoS_x composite was prepared. Firstly, the chitosan power was dissolved in acetic acid solution with volume fraction of 1.0% under stirring for 1 h to obtain the chitosan solution with the concentration of 0.5 wt. %. Then, 5 mg CNTs/MoS_x was put into 1 mL of the prepared chitosan solution and treated with ultrasound for 2 h. Finally, 0.5 mL of $HAuCl_4$ (1 mM) was added and then stirred at 80 ^oC for 1 h. With the occurrence of the pink homogeneous solution, the AuNP-CNTs/MoS_x nanocomposites were obtained through the reduction reaction of $HAuCl_4$ by chitosan at 80 ^oC.

2.3 Characterizations

The structure of the prepared CNTs/MoS_x aerogel was characterized by X-ray diffraction (XRD), high-resolution transmission electronmicroscopy (HRTEM, Tecnai F 20, FEI) and X-ray photoelectron spectroscopy (XPS) (ESCAL-ABMK II X-ray photoelectron spectrometer). A CHI660D electrochemical workstation supplied by Shanghai CH Instruments was employed for electrochemical studies. The standard three-electrode cell was used. A saturated calomel electrode (SCE) and platinum wire auxiliary electrode were used as reference and counter electrodes, respectively. All the electrochemical tests were performed at room temperature.

2.4 Preparation of PAb-AuNPs-CNTs/MoS_x nanocomposite bioconjugates

A mixture of NaOH (50 mg) and $ClCH_2COONa$ (50 mg) was added to the AuNPs-CNTs/MoSx suspension (1 mL) with the concentration of 1 mg/mL, and then treated with ultrasound for 1 h. Dilute hydrochloric acid was adopted to neutralize the resulting solution. To prepare PAb-AuNPs-

$CNTs/MoS_x$ bioconjugates, 10 mL EDC solution with the concentration of 5 mg/mL and 20 mL NHS solution with the concentration of 3 mg/mL were mixed in PBS buffer (pH 5.2) and then used to activate 400 mL AuNPs-$CNTs/MoS_x$ (0.1 mg/mL) for 30 min [26]. The mixture was separated with centrifugation and the obtained solid was washed with PBS in order to get rid of remaining EDC and NHS. The resulted solid was re-dispersed in 1 mL of PBS buffer with pH of 7.4. In order to get a homogeneous suspension, the mixture was treated with ultrasound for 5 min. Then, 1 mL of PAb with the concentration of 1 mg/mL and 2 mL of BSA with the concentration of 0.25% (w/v) were added and stirred overnight at 4 ^oC. The reaction mixture was separated with centrifugation and washed with PBS three times. The obtained solid was re-dispersed in 1.0 mL of PBS with the pH of 7.4 and kept in reserve at 4 ^oC.

2.5 Immunosensor fabrication

The glassy carbon electrode (GCE) was pretreated as follows: polished using 0.05 mm alumina, washed by distilled water and then sonicated to get rid of certain physically adsorbed substances. Subsequently, the electrode was put in an electrochemical cell and chemically cleaned with 0.05 M H_2SO_4 until the acquirement of stable background baseline. Then the electrode was treated with a thorough wash using water and dried under the protection of N_2. Soon afterwards, 6 mL of AuNPs-$CNTs/MoS_x$ solution was cast onto the surface of the obtained clean glassy carbon electrode at 25 ^oC. The obtained $CNTs/MoS_x$/GCE was rinse with water and immersed in 200 mL PBS with the pH of 7.4 containing H7-monoclonal antibodies (MAb) with the concentration of 10 mg/mL. The immobilization was conducted at 4 ^oC overnight. For the sake of avoiding non-specific adsorption on the active sites, the electrode was treated in BSA solution with the concentration of 0.25% for about 1 h at 37 ^oC to block the excess active sites. Finally, the immunosensor was successfully constructed and denoted as MAb-$CNTs/MoS_x$/GCE.

2.6 Detection of AIV H7

AIV H7 was detected by a sandwich immunoassay. Firstly, the MAb-$CNTs/MoS_x$/GCE was incubated with 100 mL of AIV H7 solution with varying concentrations for 30 min and then rinsed with PBS. Secondly, 200 mL of PAb-$CNTs/MoS_x$ bioconjugates was used to modify the electrode for 40 min and the remaining conjugates without adsorption were removed by PBS. Finally, the AgNPs was deposited on GE. The obtained electrode was employed as working electrode with platinum wire auxiliary electrode as counter electrode and SCE as reference electrode. Linear sweep voltammetry (LSV) was conducted during the potential range of 0.15 to 0.25 V at a scan rate 50 mV/s to keep a record of the currents during the detection process of AIV H7.

3. RESULTS AND DISCUSSION

The CNTs/MoS_x aerogel was synthesized via a simple solvothermal method. A mixture of $(NH_4)_2MoS_4$ and MWNTs aerogel was dissolved in DMF and heated at 200 °C for 10 h. The morphology feature of the obtained composite was characterized by TEM. As can be seen from Fig. 1A, the surface of MWNTs aerogel was successfully modified with MoS_x black dark films and the two different structures were very close to each other. MWNTs aerogel structures and they combine each other very closer, forming the layered structure of staggered, which is important to tightly attach the MoSx films on the surface of the MWNTs aerogel electrode. In the absence of carbon nanotube aerogel support, aggregated MoSx particle is produced [27]. The formation of layered and staggered structure is of great importance to the tight junction between the MoS_x films and the MWNTs aerogel. As presented in the close-up view of the gap between MoS_x nanoparticles and MWNTs aerogel (Fig. 1B), two different layered spacing can be observed: one is around 0.34 nm ascribed to the interlamellar spacing value between the graphitic planes involved in MWNTs and the other is around 0.63 nm possibly ascribed to the spacing values between the MoS_x planes.

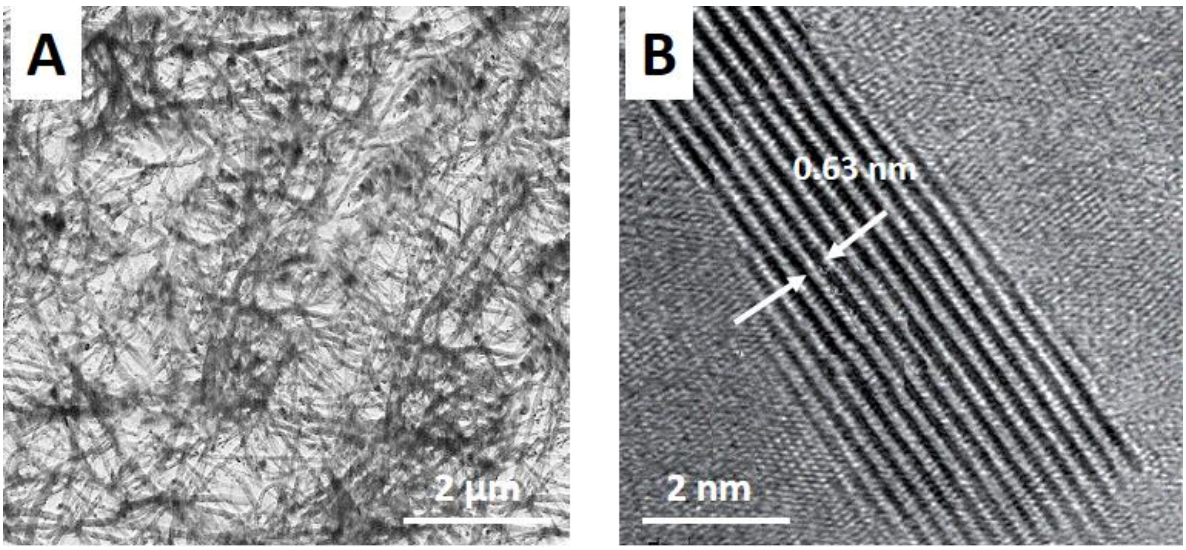

Figure 1. (A) TEM and (B) HRTEM images of CNTs/MoS_x aerogel.

The chemical states of Mo and S in the CNTs/MoS_x aerogel were measured by XPS. As presented in the high-resolution XPS spectra (Fig. 2), the binding energies located at 163.3,162.1, 232.4 and 229.2, eV were resulted from S 2p 1/2, S 2p 3/2, Mo 3d 3/2 and Mo 3d 5/2 peaks, respectively, demonstrating the existence of Mo^{4+} in the CNTs/MoS_x aerogel [28]. The higher energy shift of Mo 3d 3/2 and 3d 5/2 doublet are associated with higher valence states. The observation of Mo 3d 3/2 and Mo 3d 5/2 peaks at 233.6 and 230.5 eV with separation energies close to 3.1 eV can be

attributed to the presence of Mo^{5+} ions [29, 30]. The S 2p3/2 binding energies was occurred in doublets (161.7 and 163.2 eV), which can be resulted from apical S^{2-} or bridging disulfide S_2^{2-} ligands.

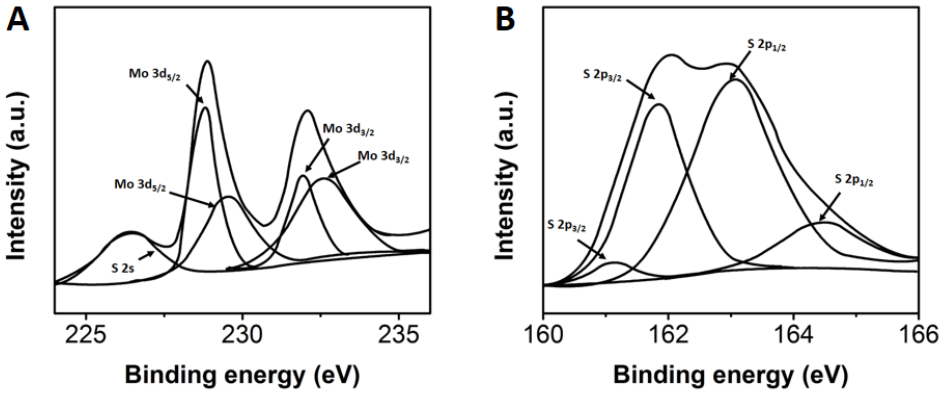

Figure 2. High resolution XPS spectra of (A) Mo 3d and (B) S 2p of CNTs/MoS_x aerogel.

The structures of MWNTs aerogel and CNTs/MoS_x aerogel were investigated by XRD. As shown in Fig. 4, the diffraction angle at $2\theta = 26.24°$ was the main characteristic peak of MWCNTs aerogel. A broad peak between $2\theta = 35°$ to 70 was observed in the XRD pattern of CNTs/MoS_x aerogel, indicating the semicrytalline nature of the obtained CNTs/MoS_x composite.

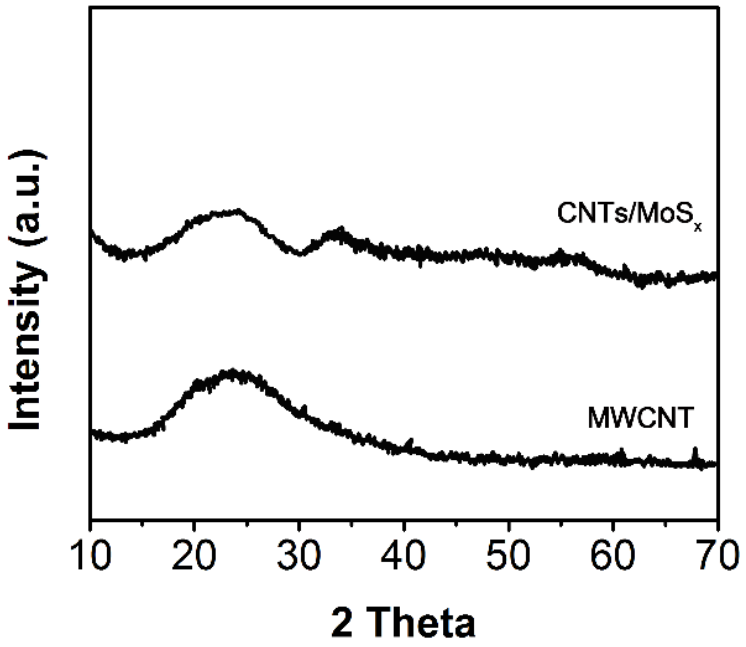

Figure 3. XRD patterns of MWNTs aerogel and CNTs/MoS_x aerogel.

The performance of the modified electrode is generally investigated by cyclic voltammetry (CV) effectively and conveniently. In our work, the electrochemical behaviours of the modified electrode after each assembly step were measured using CV technique. Fig. 4 showed the CVs of various different electrodes in 5 mM $Fe(CN)_6^{3-/4-}$ solution. For the bare GCE, a reversible CV was observed for the redox label $Fe(CN)_6^{3-/4-}$. For the CNTs/MoS_x decorated GCE, the peak current was enhancecd compared with that of bare GCE. Owing to the effective increase of active sites in the surface of the electrode by AuNPs, the GCE electrode modified with AuNPs-CNTs/MoS_x have exhibited the maximum current response. However, the peak current demonstrated a marked decrease since the immobilization of MAbs on the electrode surface, indicating the active sites for electron transfer between $[Fe(CN)_6]^{-3/-4}$ and GCE severely decreased because of the protein MAb. When BSA was employed to block non-specific sites, the peak current also decreased. What's worse, a dramatic decrease in current occurred after the contact of immunosensor with AIV H7 for 30 min. The formation of immunocomplex was the main reason for decreased current. The formed complex was inert to electrical conduction and also a blocking layer that hinders the diffusion of ferricyanide toward the electrode surface. The improved electrocatalytic activity for MoS_x/CNTs hybrids suggests the synergistic effect between 3D conductive CNTs and electroactive MoS_x nanoparticles.

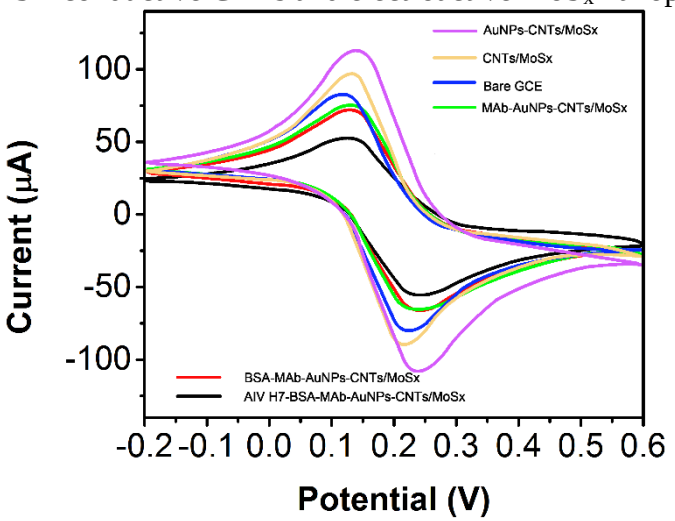

Figure 4. Cyclic voltammograms of the electrode at different stages. Scan rate 50 mV/s. Supporting electrolyte, 5 mM $Fe(CN)_6^{3-/4-}$ + 0.1 M KCl.

The linear sweep voltammetry (LSV) technique was employed to evaluate the electrochemical performances of the AIV H7 immunosensor. As depicted in the LSV plots of the BSA-MAb-AuNPs-CNTs/MoS_x-GCE (Fig. 5), only a low background current could be observed. The current at different overpotentials are quite low, which may be explained by the observation that excess loading of catalyst will increase the internal resistance. The anodic peak was unobserved during the working potential range owing to the lack of electrochemical activity substances. However, a stable anodic peak occurred

on the electrode with the adsorption of PAb-CNTs/MoS_x via sandwich immunoreactions, suggesting the excellent activity of PAb-CNTs/MoS_x bioconjugates.

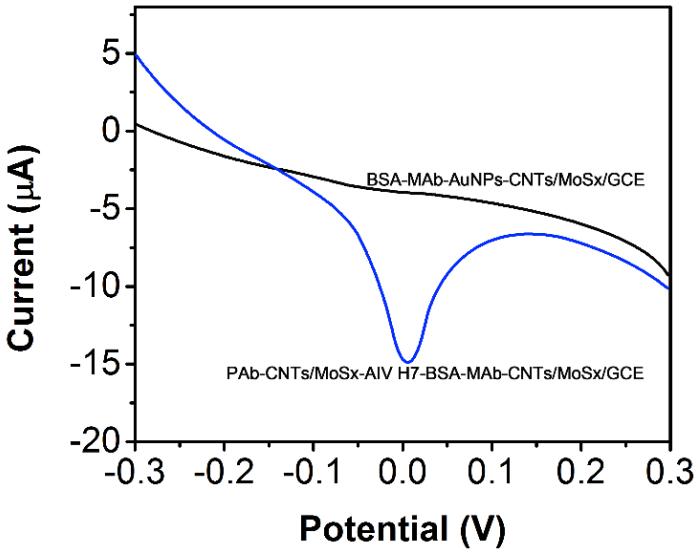

Figure 5. Linear sweep voltammetry of the immunosensor measurement process: BSA-MAb-AuNPs-CNTs/MoS_x/GCE and PAb-CNTs/MoS_x-AIV H7-BSA-MAb-CNTs/MoS_x/GCE towards 25 ng/mL H7N9.

The incubation time is of great importance for both the capture of AIV H7 and the recognition of PAb-CNTs/MoS_x. The current response increased with the increasing incubation time of AIV H7 and reached a constant value after the incubation time increased to 20 min, demonstrating the complete capture of the antigens. During the second immunoassay step, a similar trend was observed, suggesting all the antigen was saturated binded with detecting antibody.

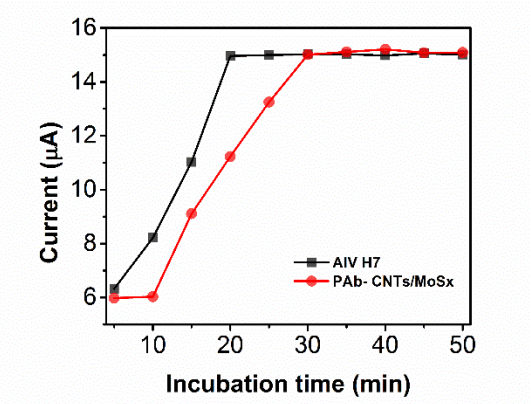

Figure 6. Influence of incubation time on the current response of immunosensor AIV H7 and PAb-CNTs/MoS_x.

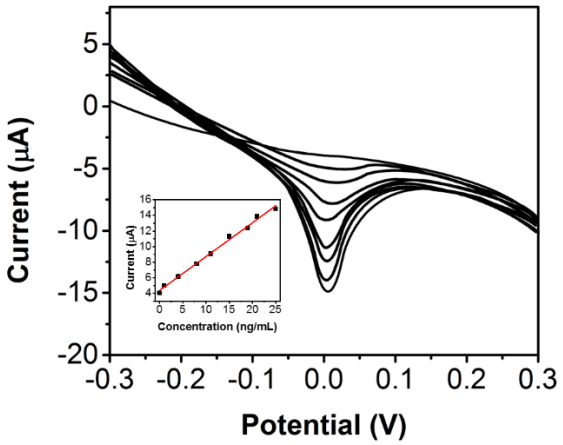

Figure 7. Typical LSV signals in the presence of different AIVH7 concentrations: from 1 to 25 ng/mL Inset: The relationship between antigen concentration and sensor response to current.

Under all the optimized conditions dissussed above, AIV H7 with varying concentrations was detected using LSV technique in the immunosensors. Five parallel experiments were carried out for each concentration. Fig. 7 showed that the LSV peak current was linearly related with the antigen concentrations ranging from 1~25 ng/mL. The linear correlation equation is $I = 4.38616 + 0.43407 C_{(AIV\ H7)}$ with the correlation coefficient 0.9958. In addition, the detection limit was 0.43 ng/mL (S/N=3). The sensitivity of the proposed method in our work far exceeded that of the traditional ELISA method. Besides, the performance of immunosensors here was about the same good as that of the reported immunosensors [31-35]. This analytical performance can be compared with those recently reported in the literature for Table 1. As compared with different determination methods, due to the high sensitivity of the proposed electrochemical performance, the PAb- CNTs/MoS_x could be used for potentially detecting AIV H7 at real samples.

Table 1. Comparison of our proposed AIV H7 electrochemical sensor with other reports.

Electrode	Linear range (μM)	Limit of detection (μM)	Reference
Serological enzyme-linked immunosorbent assay	10-50 ng/mL	2.5 ng/mL	[36]
RT-PCR	30-100 ng/mL	15 ng/mL	[5]
Multiplex RT-PCR	15-70 ng/mL	—	[4]
PCR-ELISA	7-55 ng/mL	3.66 ng/mL	[37]
PAb- CNTs/MoS_x	1~25 ng/mL	0.43 ng/mL	This work

The LSV of intra- and inter-assays was measured to evaluate the precision of immunosensor. The tests were performed for three different concentrations with each five times. As to the AIV H7

concentrations of 16, 160 and 1600 pg/mL, the precisions were 5.3, 4.7 and 4.3% for LSVs of the intra-assay and 5.7, 6.1 and 7.2% for LSVs of the inter-assay, respectively. Therefore, the precision of the immunosensors were considered acceptable, demonstrating the reproducibility of immunosensors.

The long-term stability of the prepared PAb-CNTs/MoS_x bioconjugates was investigated. The bioconjugates showed unobservable signal changes when stored in PBS with pH of 7.0 containing 0.1% NaN_3 at 4 °C for at least 2 weeks. Moreover, 91.2% of initial response was still remained after stored for 30 days. The decreased response was speculated to be caused by the deactivation of the immobilized biomolecules on the surface of PAb-CNTs/MoS_x gradually.

4. CONCLUSIONS

In conclusion, CNTs/MoS_x aerogel have been successfully prepared by a solvothermal process. A immunosensor based on PAb-CNTs/MoS_x bioconjugates was fabricated for the determination of AIV H7 with highly sensitive. A very wide linear response range (1.6×10^{-3}~16 ng/mL) and a low detection limit (1.6 pg/mL) were achieved. All the obtained results demonstrated that the immobilized MAb molecules exhibited an excellent electrochemical response to AIV H7.

ACKNOWLEDGMENTS
This work is continuously supported by the Natural Science Funds of Heilongjiang Province in China (B201422).

References

1. R. Fouchier, P. Schneeberger, F. Rozendaal, J. Broekman, S. Kemink, V. Munster, T. Kuiken, G. Rimmelzwaan, M. Schutten and G. van Doornum, *Proceedings of the National Academy of Sciences of the United States of América*, 101 (2004) 1356.
2. Y. Chen, W. Liang, S. Yang, N. Wu, H. Gao, J. Sheng, H. Yao, J. Wo, Q. Fang and D. Cui, *The Lancet*, 381 (2013) 1916.
3. H. Bao, X. Wang, Y. Zhao, X. Sun, Y. Li, Y. Xiong and H. Chen, *Journal of Virological Methods*, 179 (2012) 33.
4. Z. Xie, Y. Pang, J. Liu, X. Deng, X. Tang, J. Sun and M.I. Khan, *Molecular and Cellular Probes*, 20 (2006) 245.
5. C. Lee and D. Suarez, *Journal of Virological Methods*, 119 (2004) 151.
6. R. Collins, L. Ko, K. Fung, K. Chan, J. Xing, L. Lau and A. Yu, *Biochemical and Biophysical Research Communications*, 300 (2003) 507.
7. S. Velumani, Q. Du, B. Fenner, M. Prabakaran, L. Wee, L. Nuo and J. Kwang, *Journal of Virological Methods*, 147 (2008) 219.
8. E. Bahadır and M. Sezgintürk, *Talanta*, 132 (2015) 162.
9. R. Akter, C. Rhee and M. Rahman, *Biosensors and Bioelectronics*, 54 (2014) 351.
10. M. Yang, J. Zhang and X. Chen, *Journal of Electroanalytical Chemistry*, 736 (2015) 88.

11. Z. Zhong, W. Wu, D. Wang, D. Wang, J. Shan, Y. Qing and Z. Zhang, *Biosensors and Bioelectronics*, 25 (2010) 2379.
12. Y. Li, J. Han, R. Chen, X. Ren and Q. Wei, *Analytical Biochemistry*, 469 (2015) 76.
13. J. Huang, J. Tian, Y. Zhao and S. Zhao, *Sensors and Actuators B: Chemical*, 206 (2015) 570.
14. G. Sun, L. Zhang, Y. Zhang, H. Yang, C. Ma, S. Ge, M. Yan, J. Yu and X. Song, *Biosensors and Bioelectronics*, 71 (2015) 30.
15. B. Radisavljevic, A. Radenovic, J. Brivio, V. Giacometti and A. Kis, *Nature Nanotechnology*, 6 (2011) 147.
16. K. Chang and W. Chen, *ACS Nano*, 5 (2011) 4720.
17. T. Jaramillo, K. Jørgensen, J. Bonde, J. Nielsen, S. Horch and I. Chorkendorff, *Science*, 317 (2007) 100.
18. X. Zhong, H. Yang, S. Guo, S. Li, G. Gou, Z. Niu, Z. Dong, Y. Lei, J. Jin and R. Li, *Journal of Materials Chemistry*, 22 (2012) 13925.
19. Q. Xiang, J. Yu and M. Jaroniec, *Journal of the American Chemical Society*, 134 (2012) 6575.
20. D. Merki, S. Fierro, H. Vrubel and X. Hu, *Chemical Science*, 2 (2011) 1262.
21. S. Chen, J. Duan, M. Jaroniec and S.Z. Qiao, *Angewandte Chemie International Edition*, 52 (2013) 13567.
22. S. Lim, H. Elim, X. Gao, A. Wee, W. Ji, J. Lee and J. Lin, *Physical Review B*, 73 (2006) 045402.
23. L. Chen, C. Xu, R. Du, Y. Mao, C. Xue, L. Chen, L. Qu, J. Zhang and T. Yi, *Journal of Materials Chemistry A*, 3 (2015) 5617.
24. R. Du, N. Zhang, J. Zhu, Y. Wang, C. Xu, Y. Hu, N. Mao, H. Xu, W. Duan and L. Zhuang, *Small*, 11 (2015) 3903.
25. Y. Yan, B. Xia, X. Qi, H. Wang, R. Xu, J.-Y. Wang, H. Zhang and X. Wang, *Chemical Communications*, 49 (2013) 4884.
26. R. Raghav and S. Srivastava, *Biosensors and Bioelectronics*, 78 (2016) 396.
27. S. Reddy, R. Du, L. Kang, N. Mao and J. Zhang, *Appl. Ctatl. B-Environ.*, 194 (2016) 16.
28. V. Koroteev, L. Bulusheva, I. Asanov, E. Shlyakhova, D. Vyalikh and A. Okotrub, *J Phys Chem C*, 115 (2011) 21199.
29. M. Baker, R. Gilmore, C. Lenardi and W. Gissler, *Appl. Surf. Sci.*, 150 (1999) 255.
30. H. Wang, P. Skeldon and G. Thompson, *Surface and Coatings Technology*, 91 (1997) 200.
31. B. Mu, X. Huang, P. Bu, J. Zhuang, Z. Cheng, J. Feng, D. Yang, C. Dong, J. Zhang and X. Yan, *Journal of Virological Methods*, 169 (2010) 282.
32. A. Zhang, M. Jin, F. Liu, X. Guo, Q. Hu, L. Han, Y. Tan and H. Chen, *Avian Diseases*, 50 (2006) 325.
33. X. Zou, H. Huang, Y. Gao and X. Su, *The Analyst*, 137 (2012) 648.
34. L. Chen, Z. Sheng, A. Zhang, X. Guo, J. Li, H. Han and M. Jin, *Luminescence*, 25 (2010) 419.
35. X. Li, D. Lu, Z. Sheng, K. Chen, X. Guo, M. Jin and H. Han, *Talanta*, 100 (2012) 1.
36. G. Sala, P. Cordioli, A. Moreno-Martin, M. Tollis, E. Brocchi, A. Piccirillo and A. Lavazza, *Avian Diseases*, 47 (2003) 1057.
37. M. Munch, L.P. Nielsen, K. Handberg and P.H. Jørgensen, *Archives of Virology*, 146 (2001) 87.